Tenth International Conference on Computational Fluid Dynamics (ICCFD10), Barcelona,Spain, July 9-13, 2018

ICCFD10-2018-xxxx

Numerical Simulations of Flows Through Non-uniform Porous Media

Pradeep Kumar* and Rolf Radespiel*
Corresponding author: pradeep.kumar@tu-bs.de

* Institute of Fluid Mechanics, Technische Universität Braunschweig, Germany.

May 28, 2018

Abstract: Porous trailing edges for the wings are an active area of research to reduce the aircraft noise.Therefore, it is neccessary to predict the effect of such porous surfaces on the aerodynamics of the wings. In order to simulate the turbulent flow through the porous media, a VRANS model for flow through isotropic and uniform porous media was previously developed. This numerical model is further extended to simulate flows through non-uniform porous media. The model is verified with the help of generic test cases for laminar and turbulent flows. Numerical results are presented for a non-uniform porous medium at the trailing edge of an airfoil.

Keywords: Computational Fluid Dynamics, Turbulence Modeling, aircraft noise reduction.

Nomenclature

A_{fs}	Surface area of porous structure
c_F	Forchheimer coefficient
c_t	Modelling constant for velocity fluctuation triple correlations
E	Energy
H	Enthalpy
k_d	Thermal diffusion
n_i	i-component of the normal vector
p	Pressure
Re	Reynolds number
t	Time
u_τ	Shear stress velocity
V_B	Bulk velocity i.e. mean velocity in the free flow
v_i	Velocity in direction i
x_i	Coordinate in direction i
κ	Permeability
μ	Dynamic viscocity
ν	Kinematic viscosity
ϕ	Porosity
ρ	Density
τ_{ij}	Element i, j of tensor of viscous stresses
$\overline{\varphi}$	Time average of arbitrary variable φ
$\widetilde{\varphi}$	Density weighted time average of arbitrary variable φ
$\langle\varphi\rangle$	Volume average of arbitrary variable φ
$\langle\varphi\rangle_{\mathcal{F}}$	Density weighted volume average of arbitrary variable φ

1 Introduction

Aircraft wing noise reduction is an active area of interest for the current collaborative research center SFB880, located at the Technische Universität at Braunschweig, Germany. Porous materials have been used by Herr [1] to reduce the trailing edge noise of airplanes where a noise reduction on the order of 2-6 dB is achieved. It is expected that the introduction of porous materials would lead to change in the aerodynamic and turbulent flow behavior in and around the wings. In an attempt to numerically simulate these changes a volume and Reynolds averaged Navier-Stokes (VRANS) based numerical model is developed that can resolve the turbulent flows in and around the porous surfaces. The other possibilities such as LES and DNS are also being used within the research center, however they are computationally expensive for trying out a large number of porous materials at different flow conditions such as high Reynolds numbers. The previous VRANS model [2, 3] computes the turbulent flow over porous media with uniform and isotropic material properties. It is desirable to have the capabilities to also simulate a non-uniform and anistropic porous materials. The model is extended for nonuniform porous medium here based on Navier-Stokes (NS) equations. The additional drag due to the porous medium in the momentum equation is compensated by the Darcy and Forchheimer terms for the flow through porous media. In addition, the volume averaging procedure leads to additional terms for spatial gradients of porosities in the basic conservation laws of NS equations. Furthermore, Reynolds averaging principles are employed to model the turbulence inside the porous media. The JHh-v2 Reynolds stress model [4, 5] is extended to model the various complex terms of the Reynolds stress equations. Additional terms due to the gradients of porosity appear in the equations as compared to the original homogenous porosity numerical model [3]. The VRANS model has been implemented in the DLR-TAU code [6] .

The previous model for uniform porous materials has been extensively tested in the past using the generic test cases [2] as well as for aircraft wings [7]. The present version of the model is verified here for similar cases based on generic channel flows. The results of a numerical simulation for an airfoil with porous trailing edge with nonuniform porous material are also presented. Section 2 describes the derivations of the equations for the flow model. Section 3 outlines the setup of testcases for model verification and the numerical results for a laminar flow followed by a turbulent flow. The results of a simulation for a 2D airfoil are presented in section 4. The final section, 5, presents the conclusions and plans for the future work.

2 Numerical model

The governing volume and Reynolds averaged Navier-Stokes (VRANS) equations for the turbulent flow through a uniform and isotropic porous medium were already presented in [3, 7] in great detail. The equations have to be extended such that the effect of the variable porous properties can be accounted for the present work. Navier-Stokes equations are first volume averaged, taking into account the porosity effects by applying additional drag [8] and then time averaging also known as Reynolds averaging is applied on the resulting equations to obtain a set of VRANS equations.

2.1 Volume Averaging

The Navier-Stokes equations in the differential form in Einstein notation can be written as:

$$\frac{\partial \rho}{\partial t} + \frac{\partial \rho v_i}{\partial x_i} = 0 \tag{1a}$$

$$\frac{\partial \rho v_i}{\partial t} + \frac{\partial \rho v_i v_j}{\partial x_j} + \frac{\partial p}{\partial x_i} - \frac{\partial \tau_{ij}}{\partial x_j} = 0 \tag{1b}$$

$$\frac{\partial \rho E}{\partial t} + \frac{\partial \rho v_i H}{\partial x_i} - \frac{\partial v_i \tau_{ij}}{\partial x_j} - \frac{\partial k_{d,i}}{\partial x_i} = 0 \tag{1c}$$

where t is the time, x_i are the Cartesian coordinates, ρ is the density, v_i are the velocity components, p is the pressure, τ_{ij} is the tensor of viscous stresses, H is the total enthalpy, E is the total energy including internal energy e and the kinetic energy $\frac{v_i v_j}{2}$ and k_d is the thermal diffusion.

These equations serve here as the starting point. The volume averaging principles are defined similar to [2, 3], whereby the spatial averaging can be written as

$$\langle \varphi \rangle = \frac{1}{V_\mathrm{f}} \int\limits_{V_\mathrm{f}} \varphi \, \mathrm{d}V \tag{2}$$

with V_f being the fluid volume inside the porous structure and φ as an arbitrary variable to be averaged and the density weighted averaging is defined as

$$\langle \varphi \rangle_\mathcal{F} = \frac{1}{V_\mathrm{f} \langle \rho \rangle} \int\limits_{V_\mathrm{f}} \rho \varphi \, \mathrm{d}V = \frac{\langle \rho \varphi \rangle}{\langle \rho \rangle} \ . \tag{3}$$

Additional relations are required for the derivatives of an averaged state variable in the Navier-Stokes equations. Mößner [2] following the derivations from Bear [9] for a rigid porous structure with variable porosities ϕ shows these relations to be

$$\left\langle \frac{\partial \varphi}{\partial t} \right\rangle = \frac{\partial \langle \varphi \rangle}{\partial t} + \frac{\langle \varphi \rangle}{\phi} \frac{\partial \phi}{\partial t} \tag{4a}$$

$$\left\langle \frac{\partial \varphi}{\partial x_i} \right\rangle = \frac{\partial \langle \varphi \rangle}{\partial x_i} + \frac{\langle \varphi \rangle}{\phi} \frac{\partial \phi}{\partial x_i} + \frac{1}{V_\mathrm{f}} \int\limits_{A_\mathrm{fs}} \varphi n_i \, \mathrm{d}A \tag{4b}$$

where n_i is the i-th component of the normal vector $\vec{n}$ and A_fs is the surface area of the pores. Following these relations and neglecting the correlations between spatial deviations, spatial averaging of the Navier-Stokes equations (1) results in

$$\frac{\partial \langle \rho \rangle}{\partial t} + \frac{\partial \langle \rho \rangle \langle v_i \rangle_\mathcal{F}}{\partial x_i} + \frac{\langle \rho \rangle \langle v_i \rangle_\mathcal{F}}{\phi} \frac{\partial \phi}{\partial x_i} = 0 \tag{5a}$$

$$\begin{aligned} &\frac{\partial \langle \rho \rangle \langle v_i \rangle_\mathcal{F}}{\partial t} + \frac{\partial \langle \rho \rangle \langle v_i \rangle_\mathcal{F} \langle v_j \rangle_\mathcal{F}}{\partial x_j} + \frac{\langle \rho \rangle \langle v_i \rangle_\mathcal{F} \langle v_j \rangle_\mathcal{F}}{\phi} \frac{\partial \phi}{\partial x_j} + \frac{\partial \langle p \rangle}{\partial x_i} + \frac{\langle p \rangle}{\phi} \frac{\partial \phi}{\partial x_i} \\ &\qquad - \frac{\partial \langle \tau_{ij} \rangle}{\partial x_j} - \frac{\langle \tau_{ij} \rangle}{\phi} \frac{\partial \phi}{\partial x_j} + \frac{1}{V_\mathrm{f}} \int\limits_{A_\mathrm{fs}} p \cdot n_i - \tau_{ij} n_j \, \mathrm{d}A = 0 \end{aligned} \tag{5b}$$

$$\begin{aligned} &\frac{\partial \langle \rho \rangle \langle E \rangle_\mathcal{F}}{\partial t} + \frac{\partial \langle \rho \rangle \langle v_i \rangle_\mathcal{F} \langle H \rangle_\mathcal{F}}{\partial x_i} + \frac{\langle \rho \rangle \langle v_i \rangle_\mathcal{F} \langle H \rangle_\mathcal{F}}{\phi} \frac{\partial \phi}{\partial x_i} + \frac{\partial \langle k_{d,i} \rangle}{\partial x_i} + \frac{\langle k_{d,i} \rangle}{\phi} \frac{\partial \phi}{\partial x_i} \\ &\qquad - \frac{\partial \langle v_i \rangle_\mathcal{F} \langle \tau_{ij} \rangle}{\partial x_j} - \frac{\langle v_i \rangle_\mathcal{F} \langle \tau_{ij} \rangle}{\phi} \frac{\partial \phi}{\partial x_j} = 0 \ . \end{aligned} \tag{5c}$$

The surface integral in the momentum equation (5b) describes the additional drag inside the porous medium. It is modelled with Darcy's law extended by a quadratic relation called Forchheimer term (cf. [8]):

$$\frac{1}{V_\mathrm{f}} \int\limits_{A_\mathrm{fs}} p \cdot n_i - \tau_{ik} n_k \, \mathrm{d}A = \underbrace{\phi \frac{\mu}{\kappa} \langle v_i \rangle_\mathcal{F}}_{\text{Darcy}} + \underbrace{\phi^2 \frac{c_F}{\sqrt{\kappa}} \langle \rho \rangle \langle v_i \rangle_\mathcal{F} \cdot |\langle \vec{v} \rangle_\mathcal{F}|}_{\text{Forchheimer}} - \underbrace{\frac{\langle p \rangle}{\phi} \frac{\partial \phi}{\partial x_i} + \frac{\langle v_i \rangle_\mathcal{F} \langle \tau_{ij} \rangle}{\phi} \frac{\partial \phi}{\partial x_j}}_{\text{forces due to porosity gradients}} \tag{6}$$

with the dynamic viscosity μ, the permeability κ and the Forchheimer coefficient c_F. The momentum equation (5b) then becomes

$$\frac{\partial \langle \rho \rangle \langle v_i \rangle_\mathcal{F}}{\partial t} + \frac{\partial \langle \rho \rangle \langle v_i \rangle_\mathcal{F} \langle v_j \rangle_\mathcal{F}}{\partial x_j} + \frac{\langle \rho \rangle \langle v_i \rangle_\mathcal{F} \langle v_j \rangle_\mathcal{F}}{\phi} \frac{\partial \phi}{\partial x_j} + \frac{\partial \langle p \rangle}{\partial x_i} - \frac{\partial \langle \tau_{ij} \rangle}{\partial x_j} + \phi \frac{\mu}{\kappa} \langle v_i \rangle_\mathcal{F} + \phi^2 \frac{c_F}{\sqrt{\kappa}} \langle \rho \rangle \langle v_i \rangle_\mathcal{F} \cdot |\langle \vec{v} \rangle_\mathcal{F}| = 0 \tag{7}$$

The spatial gradient terms of the porosities $\frac{\partial \phi}{\partial x_i}$ are the additional terms to be considered in all equations when compared to the original equations for homogenous porous materials as used in [2, 3].

2.2 Reynolds Averaging

Time averaging of the compressible Navier-Stokes equations is a well known procedure for computing the mean flow instead of fully resolving the turbulent flow motion. The procedure is thoroughly described in Wilcox [10] and was discussed in detail for the uniform and isotropic porous media in the [3]. Time averaging the previously derived volume averaged Navier-Stokes equations from section 2.1 following a similar procedure and time averaging principles results in:

$$\frac{\partial \overline{\rho}}{\partial t} + \frac{\partial \overline{\rho}\widetilde{v_i}}{\partial x_i} + \frac{\overline{\rho}\widetilde{v_i}}{\phi}\frac{\partial \phi}{\partial x_i} = 0 \tag{8a}$$

$$\begin{aligned}\frac{\partial \overline{\rho}\widetilde{v_i}}{\partial t} + \frac{\partial \overline{\rho}\widetilde{v_i}\widetilde{v_j}}{\partial x_j} + \frac{\partial \overline{\rho}\widetilde{v_i''v_j''}}{\partial x_j} + \frac{\partial \overline{p}}{\partial x_i} - \frac{\partial \overline{\tau_{ij}}}{\partial x_j} + \phi\frac{\mu}{\kappa}\widetilde{v_i} \\ + \phi^2\frac{c_F}{\sqrt{\kappa}}\overline{\rho}\widetilde{v_i|\vec{v}|} + \frac{\overline{\rho}(\widetilde{v_i}\widetilde{v_j} + \widetilde{v_i''v_j''})}{\phi}\frac{\partial \phi}{\partial x_j} = 0\end{aligned} \tag{8b}$$

$$\begin{aligned}\frac{\partial \overline{\rho}\widetilde{E}}{\partial t} + \frac{\partial \overline{\rho}\widetilde{v_i}\widetilde{H}}{\partial x_i} + \frac{\partial \overline{\rho}\widetilde{v_i''H''}}{\partial x_i} - \frac{\partial \widetilde{v_i}\overline{\tau_{ij}}}{\partial x_j} - \frac{\partial \widetilde{v_i''\tau_{ij}}}{\partial x_j} + \frac{\partial \overline{k_{d,i}}}{\partial x_i} \\ + \frac{\overline{\rho}(\widetilde{v_i}\widetilde{H} + \widetilde{v_i''H''})}{\phi}\frac{\partial \phi}{\partial x_i} - \frac{(\widetilde{v_i}\overline{\tau_{ij}} + \widetilde{v_i''\tau_{ij}})}{\phi}\frac{\partial \phi}{\partial x_j} + \frac{\overline{k_{d,i}}}{\phi}\frac{\partial \phi}{\partial x_i} = 0\end{aligned} \tag{8c}$$

where $\overline{\varphi}$ and $\widetilde{\varphi}$ are the time averages and the density weighted time averages of an arbitrary quantity φ and $\varphi'' = \varphi - \widetilde{\varphi}$. A number of unknowns appear in these equations which require further derivations and modeling, however the main difference to the isotropic porous model equations is again the presence of spatial gradients of the porosities. The $\widetilde{v_i''H''}$ term can be simplified as single terms:

$$\widetilde{v_i''H''} = \widetilde{v_j''}\widetilde{v_i''v_j''} + \frac{1}{2}\widetilde{v_i''v_j''v_j''} + \widetilde{v_i''h''}$$

A second order approximation of the Forchheimer term (see [3] for details) results in:

$$\phi^2\frac{c_F}{\sqrt{\kappa}}\overline{\rho}\widetilde{v_i|\vec{v}|} \approx \phi^2\frac{c_F}{\sqrt{\kappa}}\overline{\rho}\left[\widetilde{v_i}|\widetilde{\vec{v}}| + \frac{1}{2}\frac{\widetilde{v_i}}{|\widetilde{\vec{v}}|}\widetilde{v_k''v_k''} + \frac{\widetilde{v_k}}{|\widetilde{\vec{v}}|}\widetilde{v_i''v_k''} - \frac{1}{2}\frac{\widetilde{v_i}\widetilde{v_k}\widetilde{v_l}}{|\widetilde{\vec{v}}|^3}\widetilde{v_k''v_l''}\right] . \tag{9}$$

The additional unknown variables of the Reynolds averaged volume averaged Navier-Stokes equations (8) are the Reynolds stresses $\widetilde{v_i''v_j''}$, the velocity-shear-stress correlations $\widetilde{v_i''\tau_{ij}''}$ and, the triple correlations $\widetilde{v_i''v_j''v_k''}$ and the velocity-enthalpy correlations $\widetilde{v_i''h''}$.

2.3 Turbulence modelling

In order to obtain turbulence quantities such as Reynolds stresses as required for equations (8b), the derivations of Reynolds stress equations are extensively discussed by Wilcox [10] mainly based on the formulation:

$$\overline{v_i\mathcal{N}_j + v_j\mathcal{N}_i} - \widetilde{v_i}\overline{\mathcal{N}_j} - \widetilde{v_j}\overline{\mathcal{N}_i} = 0$$

where $\mathcal{N}_i$ is the momentum equation (7) and $\overline{\mathcal{N}_i}$ is the Reynolds averaged momentum equation (8b). The derivation of Reynolds stress equations inside the porous regions leads to the following additional terms:

$$\mathcal{P}_{\mathrm{RS}ij,\mathrm{Darcy}} = -\phi\frac{\mu}{\kappa}\left[\overline{v_i''}\widetilde{v_j} + \overline{v_j''}\widetilde{v_i} + 2\widetilde{v_i''v_j''}\right] \tag{10a}$$

$$\mathcal{P}_{\mathrm{RS}ij,\mathrm{Forch}} = -\frac{\phi^2 c_F}{\sqrt{\kappa}}\overline{\rho}\left(\widetilde{v_i''v_j|\vec{v}|} + \widetilde{v_j''v_i|\vec{v}|}\right) \tag{10b}$$

$$\mathcal{P}_{\mathrm{RS}ij,\mathrm{gradients}} = \frac{\overline{\rho}}{\phi}\frac{\partial \phi}{\partial x_k}\left(\widetilde{v_i''v_j''v_k''} + \widetilde{v_j''v_k''v_i''} + \widetilde{v_k''v_i''v_j''} + \widetilde{v_i''v_j''v_k''}\right) \tag{10c}$$

which have to be added to Reynolds stress equations. In this work, the terms are modelled similar to the *JHh-v2* turbulence model. This Reynolds stress model was first presented by Jakirlic and Hanjalic [4, 5] and uses the homogeneous dissipation rate ε^h as the length scale variable. Recently, Ccora et al. [11] recalibrated several parameters for better performance in transonic flow applications to attain version *v2*. The triple correlations in equation (10c) are modelled by the model of Hanjalic and Launder [12]

$$\widetilde{v_i''v_j''v_k''} = c_t\frac{k}{\varepsilon^h}\left[\widetilde{v_i''v_l''}\frac{\partial\widetilde{v_j''v_k''}}{\partial x_l} + \widetilde{v_j''v_l''}\frac{\partial\widetilde{v_i''v_k''}}{\partial x_l} + \widetilde{v_k''v_l''}\frac{\partial\widetilde{v_i''v_j''}}{\partial x_l}\right] \tag{11}$$

with the modelling constant c_t and the turbulent energy $k = \frac{\widetilde{u_i''u_i''}}{2}$. The other unknown term $\widetilde{v_i''h''}$ is modelled similar to the nonporous regions as:

$$\overline{\rho}\widetilde{v_k''h''} = -c_p\lambda_t\frac{\partial\overline{T}}{\partial x_k} \tag{12}$$

where the turbulent thermal conductivity $\lambda_t = \frac{\mu_t}{\sigma_t}$, μ_t is the turbulent eddy viscosity and σ_t is the turbulent Prandtl number. This formulation limits the model as the gradients of temperature due to the presence of porous structures are ignored. Note that a closure the Forchheimer term in equation (10c) is not provided in this text as it has been thoroughly covered in previous publications [2, 3]. The remaining unknown variable $\overline{v_i''\tau_{ij}}$ is neglected. It is to be noted here that a special interface treatment is required for the grid points where the porosity jumps from a smaller number to 1 in the nonporous region. This includes a calculation based on the isentropic change in the flow properties at the interface and conversation of the mean flow fluxes as well as momentum fluxes due to turbulence as discussed in [3] in details.

The additional terms based on the porosity gradients as obtained in the equations (5) and (8) are implemented in the finite-volume method based flow solver DLR-TAU code.

3 Verification of Numerical Model with generic channel cases

Two test cases based on channels are presented here for investigating the present model. The first test case would focus on verification of the basic laminar flow through the channel compared with an analytical solution for the same. The second test case with nonuniform porous media in the bottom half would be used to analyze the turbulent properties.

3.1 Laminar flow Through a Channel

The setup for a channel with porous blockage is shown in Figure 1. The boundary conditions are set to slip walls at the top and bottom of the channel, and a set of inflow-outflow conditions driving the flow in x-direction. A similar test case was previously presented [3] for the verification of Darcy and Forchheimer contributions for a uniform porous media. For the purpose of current work, the porous block has a constant porosity $\phi = 0.5$ for the first half and the porosity ϕ increases linearly to $\phi = 0.75$ by the end of the porous block. The Darcy number is $Da = \frac{\kappa}{L^2} = 1 \cdot e^{-5}$ for the porous medium and the Forchheimer coefficient is $C_F = 0$ i.e. the contribution of the Forchheimer term is neglected for simplification purposes. The inflow conditions are Mach number $Ma = 0.02$ and Reynolds number $Re = 200000$. The solution is shown in Figure 2. The velocity distribution along the length of the channel is normalized with the inflow velocity v_0 and the pressure difference $(\overline{p} - p_0)$ is normalized by the inflow dynamic pressure $0.5\rho_0 v_0^2$. The analytical solution for the velocity is obtained from the continuity equation [5a] which reduces to

$$\frac{\partial v_x}{\partial x} = -\frac{v_x}{\phi}\frac{\partial \phi}{\partial x} \tag{13}$$

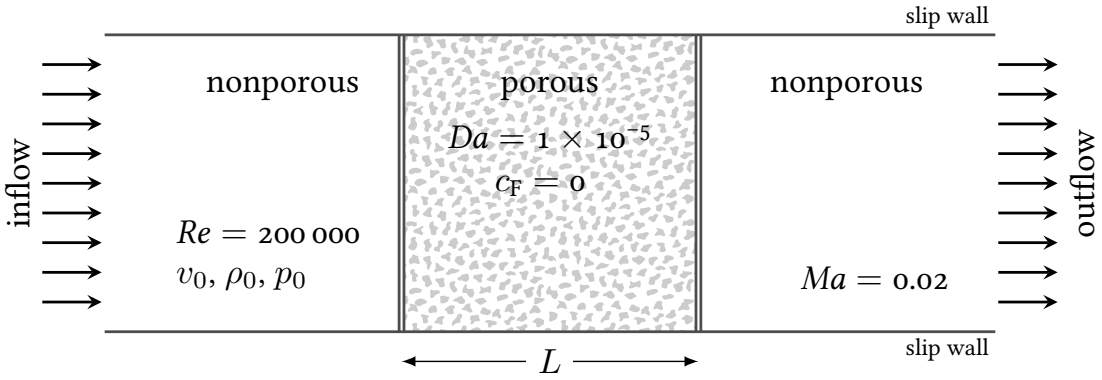

Figure 1: Numerical setup for a laminar channel case with porous blockage.

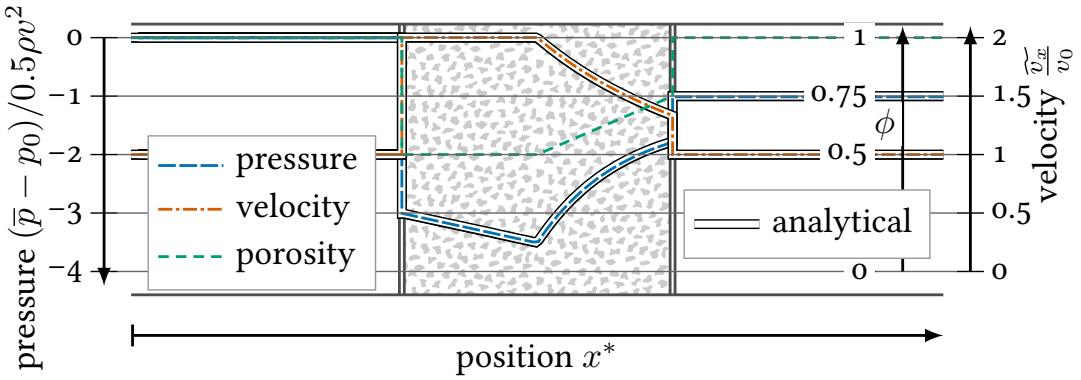

Figure 2: Porosity, velocity and pressure distribution along the laminar channel with porous blockage.

for such incompressible flows. Since $\frac{\partial \phi}{\partial x}$ is a constant, it is fairly easy to solve the equation 13 analytically. The pressure distribution is obtained from the momentum equation [7] which simplifies to the following form:

$$\frac{\partial p}{\partial x} = -\phi \frac{\mu}{\kappa} v_x - \frac{\rho v_x^2}{\phi} \frac{\partial \phi}{\partial x} \tag{14}$$

The analytical solution for the velocity and pressure is also shown in Figure 2 which matches the numerical solutions obtained from the flow solver TAU very well.

3.2 Turbulent flow Through a Channel

The previous testcase verifies the model for a laminar flow, whereas analysis for turbulent flow is presented here. We seek a generic test case with non-uniform porosity. However, an experimental or numerical database for verification is not available to the best of the knowledge of authors. Therefore a variation of the validation case from the previous work [3] is considered here. The resolved DNS computation for a generic channel case called CUB by Breugem [8] were used previously for validations where lower half of the channel is filled with porous material defined by a grid of cubes. The setup for this channel is shown in Figure 3 where the height and length of the channel are $2H$ x $5H$ and the interface between porous and nonporous media is at $0.9H$. The material properties for the uniform porous medium for the CUB testcase are given as porosity $\phi = 0.875$, Darcy number $Da = 3.4e^{-4}$, and Forchheimer coefficient $c_F = 0.026$.

For the current work, the porosity is linearly increased from $\phi = 0.875$ at $z/H = 0.70$ to $\phi = 1.0$ at $z/H = 0.9$ in order to simulate a testcase where the porous medium gradually turns into freeflow before the interface. This should in effect turn off the interface jump of the solution, which was required for the numerical model in the previous validation cases where the porosity jumps from $\phi = 0.875$ to 1.0 at this

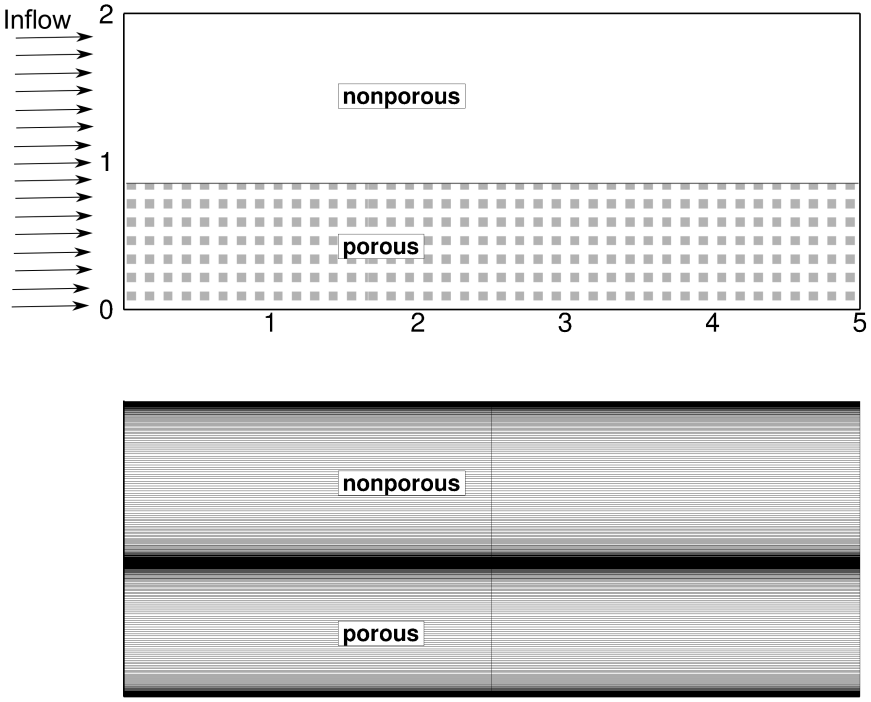

Figure 3: Numerical setup (above) and the grid (below) for the generic channel with turbulent flow.

interface. Note that, the permeability κ changes with porosity ϕ are modelled in the region of interest according to the following equation:

$$\kappa = C_{kc}\frac{\phi^3}{(1-\phi)^2}$$

where C_{kc} is a constant. This relationship is known as Kozeny-Carman (KC) model[13, 14]. Although this equation is only valid for incompressible laminar flow, it is here considered to systematically model the permeability in order to accomodate the proposed porosity variations inside the porous medium. Alternatively, a previously known linear distribution of permeabilities can also be supplied to the flow solver. Here, $C_{kc} = 7.93e^{-6}$ based on the uniform porosity and permeability below the variable porosities. The numerical grid is shown in Figure 3 with 360 points along the channel height. The grid-spacing at the wall is kept so that $y^+ < 1$ near the walls and at the interface.

The Reynolds number is defined as $Re = \frac{HV_B}{\nu} = 5500$ where H is the free flow height, V_B is the average velocity inside the free flow and ν is the kinematic viscosity. The average flow velocity V_B in the free flow channel region is set according to a Mach number $Ma = 0.15$. The velocity profile from the VRANS simulations for the testcase is compared with the uniform porous medium case in Figure 4. A higher velocity at and around the interface is observed as expected in this case as the $0.2H$ before the interface is more porous than the CUB case with constant porosity. It can also be seen that the CFD solutions from the variable porosities are in good agreement around the maximum of the free flow and also along the lower part of the porous medium. This is also expected since the flow velocity far away from the non-uniform porosity should eventually be the same for both cases. This trend also continues in the Reynolds stress distributions as shown in Figure 4, here the Reynolds stresses are normalized by the shear stress velocity u_τ of the upper channel wall. The shear stress velocity is defined as $u_\tau = \sqrt{\nu \left| \frac{\partial v_x}{\partial y} \right|}$. The normal Reynolds stresses R_{xx} along the flow direction as seen in Figure 4 is smaller compared to the case with a constant porous medium. This is due to 1.3 times higher gradients of the x-velocity at the interface for the latter case, leading to larger values of normal stresses along the flow direction, as the source term in the stress equation is larger. However, the

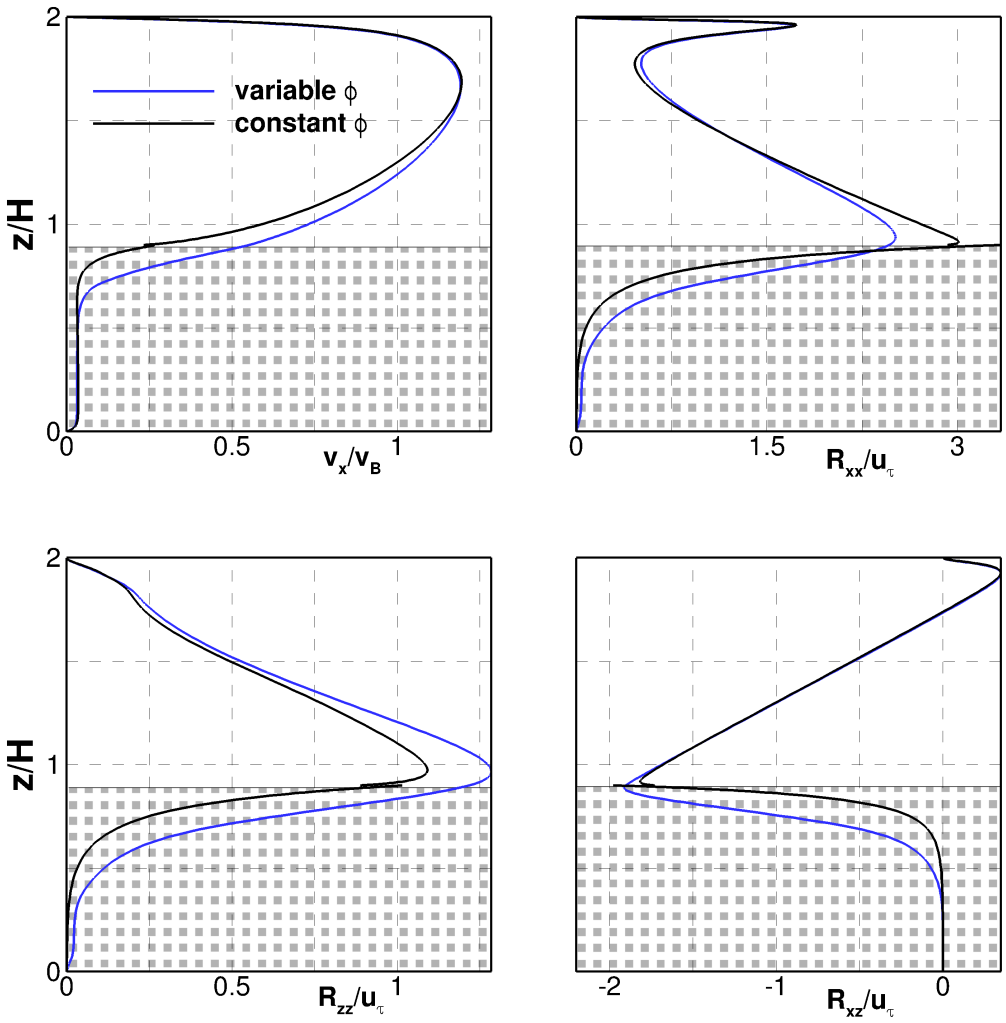

Figure 4: The velocity, normal and shear Reynolds stresses distributions along the channel height

normal stresses along the channel height R_{zz} are larger for the variable-ϕ solution. This is obviously caused by a local change in the Reynolds-stress redistribution term, where damping caused by partially solid wall is taken into account in the original model[3]. As a result of the different behaviours observed for streamwise and wall-normal stresses, the Reynolds shear stress R_{xz} remains approximately the same at the interface. We conclude that introducing a local zone of varying porosity at a porous surface has a strong effect on stress anisotropy.

The behaviour of the turbulent flow in the channel appears to be appropriate as implemented in the flow solver TAU-Code.

4 Simulations of an airfoil with porous trailing edge

2D VRANS simulations are performed for the DLR F16 airfoil to show the capability of the numerical model to simulate the flow around the airfoil with a porous trailing edge. The numerical and experimental results for the setup with uniform porous media were presented previously in [7]. The computational grid as shown in Figure 5 is an O-type mesh with sufficient cell spacing at the walls in order to resolve the boundary layer for $Re = 1,000,000$ at flow Mach number $Ma = 0.15$. The last 10 % of the airfoil is porous and this porous

trailing edge is meshed according to the spacing of the nonporous mesh. Total number of resulting grid points for the 2D simulation is ≈ 175000. The porous material considered in the previous study was derived from porous aluminium PA 80-110 with the properties: porosity $\phi = 0.46$, permeability $\kappa = 1.24e^{-10}$ and Forchheimer coefficient $C_F = 0.1$. For the present case, the porosity is linearly varied from $\phi = 0.46$ to $\phi = 1.0$ from the beginning to the end of the porous trailing edge. The permeability varies according to the KC-model with $C_{KC} = 3.7e^{-10}$ along the length of the porous part. The results from the simulations for

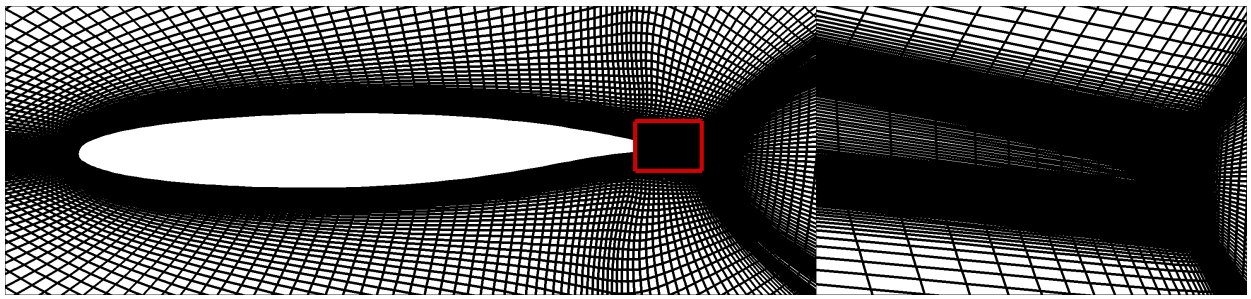

Figure 5: Numerical grid for 2D simulations of flow around DLR F16 airfoil with the porous trailing edge (insert and right).

this synthetic material are shown in Figure 6 and Figure 7 compared with the uniform porous material PA 80-110. Figure 6 shows the c_p distribution around the airfoil and at the porous trailing egdes at an angle of attack $\alpha = 6^o$. The flow motion from the pressure side through the porous medium can be seen by inspecting the streamlines. The large differences are expected as the non-uniform medium gradually turns more porous along the airfoil trailing edge, allowing a larger flow velocity along the vertical-direction. This momentum exchange separates the flow earlier on the suction side of the airfoil leading to a 7% reduction in the lift coefficient C_L as compared to the homogenous porous material PA 80-110. The turbulence distributions, based on Reynolds stresses $\frac{R_{xx}+Rzz}{v_\infty^2} = \frac{\overline{v_x''v_x''}+\overline{v_z''v_z''}}{v_\infty^2}$ are shown in Figure 7 for the same angle of attack $\alpha = 6^o$. The absence of turbulence inside the porous media is a well documented phenomenon [7] as a result of strong Darcy and Forchheimer terms damping out all the turbulence there. A slightly higher turbulence is seen in the wake of the airfoil for the non-uniform porous medium.

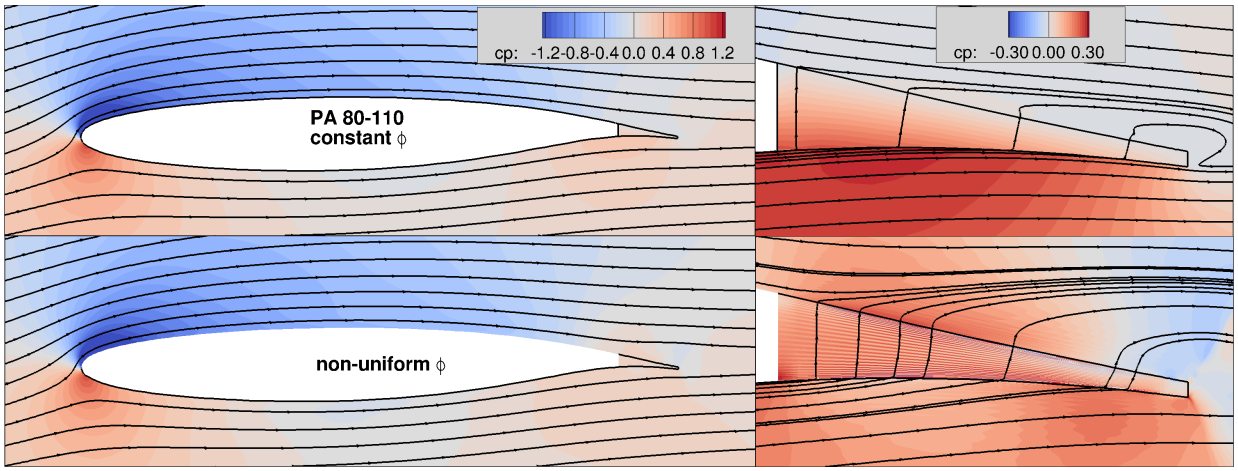

Figure 6: Pressure (c_p) distribution and streamlines around the airfoil (left) and the porous trailing edge (right) for the uniform and non-uniform porous media at an angle of attack $\alpha = 6^o$.

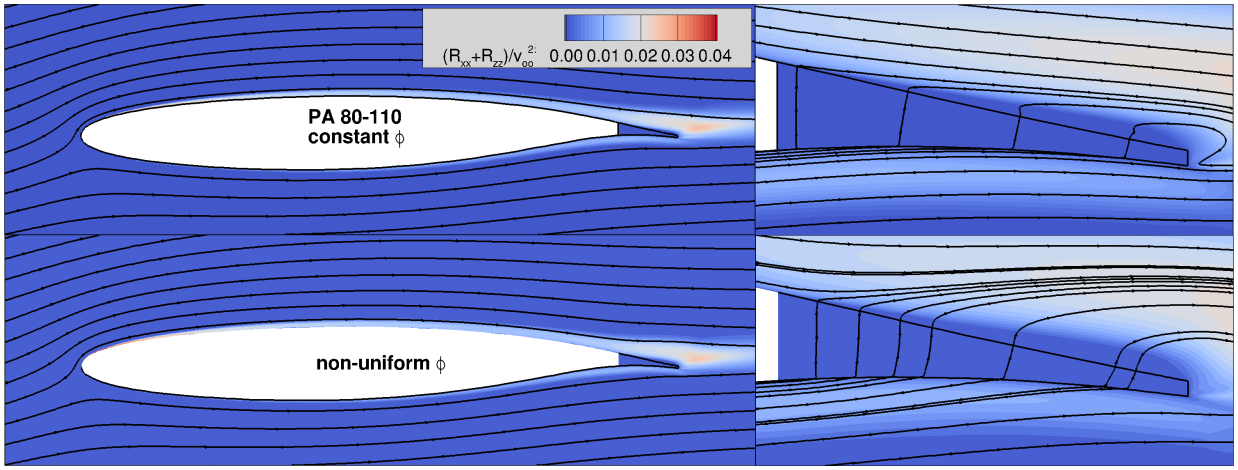

Figure 7: Turbulence distribution around the airfoil(left) and the porous trailing edge (right) for the uniform and non-uniform porous media at an angle of attack $\alpha = 6^o$.

5 Conclusion and Future Work

A set of equations are derived based on volume and Reynolds averaging (VRANS) model for simulations of turbulent flow through non-uniform porous media. The resulting additional terms in the flow equations represent the gradients of porosity. The extended equations are implemented in a flow solver for the prediction of aeronautical flows. Numerical simulations of generic test cases provide a verification for the model. Further datasets are needed at this point to validate the model for turbulent flows. LES simulations for a channel with turbulent flow through a non-uniform porous medium are foreseen in future works of the collaborative research center SFB 880. Experimental campaigns for wings with porous trailing edges are also planned in future to provide data for validating the model. Since a non-uniform porous material in practice would likely be anisotropic, the numerical model needs to be extended to anisotropic permeabilities and Forchheimer coefficients inside the porous medium.

Acknowledgement

This work was funded by the Deutsche Forschungsgemeinschaft DFG (German Research Funding Organization) in the framework of the collaborative research centre SFB 880. The authors gratefully acknowledge support from numerous discussions with Michael Mößner about the simulation concept and its implementation into code.

References

[1] M. Herr, K.-S. Rossignol, J. Delfs, M. Mößner, and N. Lippitz. Specification of porous materials for low-noise trailing-edge applications. In *20th AIAA/CEAS Aeroacoustics Conference, AIAA-2014-3041*, Atlanta, Georgia, 6 2014.

[2] M. Mößner. In *Volume-Averaged RANS-Simulation of Turbulent Flow over Porous Media. NFL Forschungs-bericht ISBN 978-3-928628-79-2*. Ph.D. Thesis, 2016-01.

[3] M. Mößner and R. Radespiel. Modelling of turbulent flow over porous media using a volume averaging approach and a Reynolds stress model. *Computers & Fluids*, 108:25–42, 2015.

[4] S. Jakirlic and K. Hanjalic. A new approach to modelling near-wall turbulence energy and stress dissipation. *Journal of Fluid Mechanics*, 459:139–166, 2002.

[5] S. Jakirlic. A DNS-based scrutiny of RANS approaches and their potential for predicting turbulent flows, 10 2003. Habilitationsschrift, Technische Universität Darmstadt.

[6] D. Schwamborn, T. Gerhold, and R. Heinrich. The DLR TAU-code: Recent applications in research and industry. In P. Wesseling, E. Oate, and J. Priaux, editors, *ECCOMAS CFD 06*. TU Delft, The Netherlands, 9 2006.
[7] M. Mößner and R. Radespiel. Flow simulations over porous media - comparisons with experiments. *Computers & Fluids*, 154:358–370, 2017.
[8] W. P. Breugem and B. J. Boersma. Direct numerical simulations of turbulent flow over a permeable wall using a direct and a continuum approach. *Physics of Fluids*, 17:1–15, 2005.
[9] J. Bear and Y. Bachmat. *Introduction to modeling of transport phenomena in porous media*, volume 4 of *Theory and applications of transport in porous media*. Kluwer Academic Publishers, 1990.
[10] D. C. Wilcox. *Turbulence Modeling for CFD*. DCW Industries, 3 edition, 2006.
[11] R.-D. Cecora, B. Eisfeld, A. Probst, and R. Radespiel. Differential Reynolds-stress modeling for aeronautics. *AIAA Journal*, 53(3), 2014.
[12] K. Hanjalic and B. E. Launder. Contribution towards a Reynolds-stress closure for low-Reynolds-number turbulence. *Journal of Fluid Mechanics*, 74:593–610, 1976.
[13] P. Carman. Fluid flow through a granular bed. *Trans. Inst. Chem. Eng.*, 15:150–167, 1937.
[14] J. Kozeny. page 271 306, 1927.